Three-dimensional boundary element formulation of an incompressible viscoelastic layer of finite thickness applied to the rolling resistance of a rigid sphere

Gérard-Philippe Zéhil[a,*], Henri P. Gavin[a]

[a]*Department of Civil and Environmental Engineering, Duke University, 121 Hudson Hall, Box 90287, Research Drive, Durham, NC 27708-0287, United States*

Abstract

A three-dimensional boundary element formulation of an incompressible viscoelastic layer of finite thickness is proposed, in a moving frame of reference. The formulation is based on two-dimensional Fourier series expansions of relevant mechanical fields in the continuum of the layer. The linear viscoelastic material is characterized, in the most general way, by its frequency-domain master curves. The presented methodology results in a compliance matrix for the layer's upper boundary, which includes the effects of steady-state motion and can be used in any contact problem-solving strategy. The proposed formulation is used, in combination with a contact solver, to build a full three-dimensional model for the steady-state rolling/sliding resistance incurred by a rigid sphere on the layer. Energy losses include viscoelastic damping and surface friction. The model is tested and its results are found to be consistent with existing solutions in limiting cases. An example is explored and the corresponding results are used to illustrate the influence of different parameters on the rolling resistance. General aspects of previously-described dependences are confirmed.

Keywords: Rolling resistance, boundary element method, viscoelastic layer, hysteretic friction, Coulomb's friction, Fourier series.

1. Introduction

For diverse reasons, rolling resistance remains important to many engineering applications. From nanotechnologies and molecular dynamics (e.g. Lee et al., 2009) to various scale industrial applications and transportation purposes (e.g. Hall, 2001; Qiu, 2006, 2009), from earthquake hazards mitigation, to energy harvesting and sustainable development considerations (e.g. Sharp, 2009), depending on human's objectives and goals, rolling resistance may be fiercely avoided or eagerly sought and thus requires careful attention.

Rolling resistance has been, and still is, widely addressed in scientific literature. In 1785 experiments on friction were reported by Coulomb (1821) and Vince and Shepherd (1785). Further experiments led to significant progress during the 1950's and the early 1960's towards a better understanding of its complex nature, involving surface contact phenomena as well as bulk properties of the interacting materials (Greenwood et al., 1961; Tabor, 1955). Hysteretic friction in the bulk is revealed in many works on nonstationary viscoelastic contact problems, in various settings (e.g. Barber et al., 2008; Chertok et al., 2001; Galin and Gladwell, 2008; Golden and Graham, 2001; Morland, 1967, 1968; Wang and Knothe, 1993). In particular, rolling friction of hard cylinders was approached in two dimensions using various methods (e.g. Hunter, 1961; Johnson, 1985; May et al., 1959; Morland, 1967; Pőschel et al., 1999) and its dependence upon physical parameters was modeled based on simplifying assumptions regarding the description of the foundation layer and/or the nature of contact interactions. A one-dimensional treatment of a hard sphere rolling on a viscoelastic half-space modeled using a 'Winkler' approximation was given by Flom and Bueche (1959). In the

*Corresponding author
Email address: gerard.zehil@duke.edu (Gérard-Philippe Zéhil)

absence of surface friction, a "first-principle" (i.e. free of empirical parameters) continuum-mechanics expression of the rolling resistance coefficient was derived by Brilliantov and Pőschel (1998) for the rolling motion of a viscoelastic sphere on a hard plane, in quasi-static conditions, such that the total stress field may be considered as the sum of an elastic part and a dissipative part, and the vertical displacement field may be approximated by the corresponding result of the static problem.

More recently, numerical difficulties associated with enforcing frictional conditions on finite element models of hyperelastic tires rolling in steady state conditions on rigid surfaces, were tackled by Laursen and Stanciulescu (2006) and Stanciulescu and Laursen (2006). A full two-dimensional boundary element formulation for a hard cylinder rolling on a viscoelastic layer of finite thickness was introduced by Qiu (2006) while Persson (2010) presented an approach to calculate the rolling resistance of hard objects on viscoelastic solids using a static pressure distribution. Alternative approaches to estimating the viscoelastic rolling resistance on a sphere in 3D are presented by Zéhil and Gavin (2013b). More comprehensive solutions to the problem of rolling resistance in three dimensions, including frictional effects, remain however in need. Furthermore, the increasing complexity of numerical models requires investigating possible ways of reducing their computational costs and hence improving their efficiency.

In this paper, we present a three-dimensional boundary element formulation of an incompressible linear viscoelastic layer of finite thickness, in a moving frame of reference. This formulation is applied, in combination with a contact solver, to build a full three-dimensional model for the resistance incurred by a rigid object (sphere) rolling/sliding on the layer, including surface friction. Inspired by the seminal work of Qiu (2006), we expand relevant mechanical fields in the continuum of the layer into two-dimensional Fourier series. The storage and loss moduli characterizing the constitutive behavior of linear viscoelastic materials, in the frequency domain, are used to relate the Fourier coefficients. The proposed formulation results in the assembly of a compliance matrix $\mathbf{C}$ characterizing the behavior of the layer's upper boundary, including the effects of steady-state motion. This compliance matrix may be used in any stationary or steady-state rolling/sliding contact problem-solving strategy. The proposed formulation is quite general and practical in that it accommodates any linear viscoelastic model, including experimental master-curves. In order to increase its computational efficiency, special attention is given to exploiting configurational similarities as well as symmetry.

2. Defining rolling resistance

Figure 1 shows a round rigid object (cylinder or sphere of center C and radius R) rolling in steady-state conditions, on a viscoelastic layer of finite thickness H. The object moves in direction x at a constant linear velocity V_s while rotating about its axis at a rotational speed Ω. It is subjected to a vertical load P (positive downwards), a driving horizontal force Q (positive in the direction of increasing x) and a driving torque T (positive clockwise). The indentation d corresponds to the maximum penetration of the rolling object below the surface of the unloaded layer.

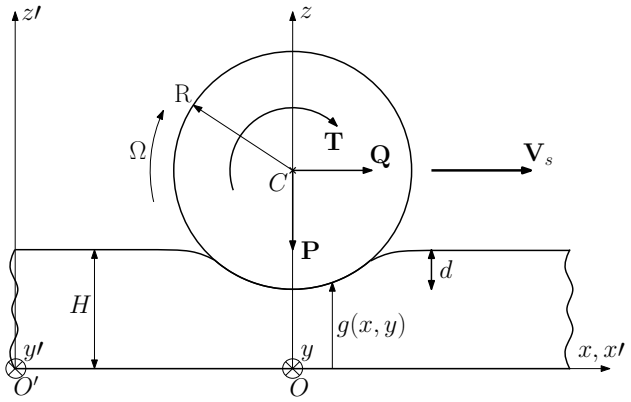

Figure 1: General model and coordinate systems

Because the contact surface takes the form of the rigid object, tangential shear stresses are circumferential and normal stresses are radial, with respect to a polar coordinate system centered at point C. However, contact stresses

can be re-expressed in the Cartesian coordinate system $Oxyz$ as well.

For the purposes of this work, rolling resistance is defined as a conceptual horizontal resisting force R_r, expressed as a positive quantity. If it were to be applied at the axis of the moving object, the rolling resistance would dissipate energy at a rate that is equivalent to the power dissipation actually incurred by the system. Rolling resistance R_r is related to Q and T by

$$R_r = Q + \frac{T\Omega}{V_s}. \tag{1}$$

In equation (1), R_r is the rolling resistance corresponding to the total dissipated power. It is considered here that, in the absence of surface friction, rolling resistance is entirely due to viscous dissipations in the bulk. In such cases, the value of a driving torque is indeterminate, as it can not be equilibrated, and rolling resistance is equal to the sum of the horizontal projection of the radial contact forces. Because of the asymmetry of these forces, the rolling resistance is non-zero.

In the presence of friction, the interfacial shear stresses are not zero and a driving torque T can be balanced by either taking the moment of the tangential contact forces about the roller axis, or taking moments of the vertical and horizontal components of the contact forces about the same axis. Surface frictions influence rolling resistance in two ways: (i) directly, by means of their resisting work localized in the slipping regions of the contact surface, and (ii) indirectly, as demonstrated by Munisamy et al. (1991), by modifying the (frictionless) contact pressure distribution, which further impacts the global energy balance. The contribution of slipping friction to rolling resistance may be evaluated as follows

$$R_r^F = \frac{1}{V_s}\int_{A_c} \mathbf{w}_t.\boldsymbol{\tau}_t dA, \tag{2}$$

where A_c stands for the contact area, $\mathbf{w}_t$ is the local tangent differential speed between the sphere and the foundation layer and $\boldsymbol{\tau}_t$ corresponds to the tangent stress field across the contact interface. In the presence of friction, the rolling resistance attributed to the viscoelastic behavior of the layer, is obtained by subtraction

$$R_r^V = R_r - R_r^F. \tag{3}$$

A common case is when the horizontal driving force Q is applied at the top of the moving object, thus generating a dependent torque $T = QR$. Substituting into expression (1) yields

$$R_r = Q(1 + \frac{R\Omega}{V_s}). \tag{4}$$

3. Governing equations

Following the development of Qiu (2006), the viscoelastic layer of thickness H is assumed to be incompressible, sustains small deformations and behaves linearly. As shown in figure 1, $Oxyz$ corresponds to a moving coordinate system traveling with the sphere, while $O'x'y'z'$ remains at rest. Both coordinate systems are related according to

$$x = x' - V_s t, \qquad y = y', \qquad \text{and} \qquad z = z'. \tag{5}$$

Also, in the traveling coordinate system, material derivatives are expressed such that time becomes an implicit variable

$$\frac{D}{Dt} = -V_s\frac{\partial}{\partial x} \qquad ; \qquad \frac{D^2}{Dt^2} = V_s^2\frac{\partial^2}{\partial x^2}. \tag{6}$$

The equilibrium equations for the elastomer in $O'x'y'z'$ are given, in tensorial form, by

$$\rho\frac{D^2\mathbf{u}}{Dt^2} = \mathbf{div}'(\mathbf{s}) - \mathbf{grad}'(p), \tag{7}$$

where $\mathbf{u} =< u, v, w >^T$ is the displacement field, ρ stands for the material's density, p is the pressure and $\mathbf{s}$ denotes the stress deviator. Equation (7) may be expressed in $Oxyz$ using (6) and hence becomes

$$\rho V_s^2\frac{\partial^2\mathbf{u}}{\partial x^2} = \mathbf{div}(\mathbf{s}) - \mathbf{grad}(p). \tag{8}$$

The constitutive behavior of the incompressible viscoelastic material may be described using the following general integral equations (e.g. Flügge, 1975; Lakes, 2009)

$$\mathbf{s}(t) = 2\int_{-\infty}^{t} G(t-s)\frac{d\boldsymbol{\epsilon}(s)}{ds}ds, \tag{9}$$

where $G(t)$ is the shear relaxation modulus of an isotropic elastomer and $\boldsymbol{\epsilon}$ corresponds to the small-stain tensor. Due to incompressibility, trace($\boldsymbol{\epsilon}$) = 0.

4. Boundary conditions

It is assumed that the foundation strip is fully adherent to its rigid subbase, which implies boundary conditions on the displacements at $z = 0$

$$\mathbf{u}(x, y, z = 0) = 0, \quad \forall(x, y). \tag{10}$$

Upper boundary conditions for the elastomer are determined by the contact problem occurring at the interface between the moving object and the foundation. The normal contact boundary conditions are expressed as

$$H + w(x, y, z = H) < g(x, y) \quad \text{if} \quad \sigma_z = 0, \tag{11}$$

$$H + w(x, y, z = H) = g(x, y) \quad \text{if} \quad \sigma_z < 0, \tag{12}$$

where, designating by z_c the coordinate of point C on the z-axis (see figure 1), $g(x, y)$ corresponds to an analytical expression for the lower surface of the moving object, i.e. for a sphere

$$g(x, y) = z_c - \sqrt{R^2 - x^2 - y^2}. \tag{13}$$

In small deformations, using equation (6), the horizontal components of the differential speed in directions x and y are given by

$$w_{tx} = V_s\left(1 + \frac{\partial u}{\partial x}\right) - R(y)\Omega, \quad \text{where} \quad R(y) = \sqrt{R^2 - y^2}, \tag{14}$$

$$w_{ty} = V_s\left(\frac{\partial v}{\partial x}\right). \tag{15}$$

The tangential contact boundary conditions involve the coefficient of sliding friction μ for the interface, as well as the components w_{tx} and w_{ty} of the differential speed, across the contact area

$$\tau_{xz}^2(H) + \tau_{yz}^2(H) < \mu^2\sigma_z^2(H) \qquad \text{if} \quad w_{tx}^2 + w_{ty}^2 = 0, \tag{16}$$

$$\tau_{xz}^2(H) + \tau_{yz}^2(H) = \mu^2\sigma_z^2(H) \qquad \text{otherwise.} \tag{17}$$

Inequality (16) applies in stick-contact conditions (i.e. in the case of an absence of relative movement between touching points) while equality (17) prevails at contact points where slipping occurs. In the latter case, following Coulomb's law of friction, the orientation of the limiting tangential contact stress must be consistent with the direction of relative movement. This additional slip-contact condition may be expressed by the constraint

$$\tau_{xz}w_{ty} - \tau_{yz}w_{tx} = 0. \tag{18}$$

Because the present three-dimensional case is treated using two-variable Fourier series, the following periodic boundary conditions are introduced, in both horizontal directions x and y for all the physical quantities ψ involved in the problem

$$\psi(x, y, z) = \psi(x + L_x, y, z), \quad \forall(x, y), \tag{19}$$

$$\psi(x, y, z) = \psi(x, y + L_y, z), \quad \forall(x, y). \tag{20}$$

Geometrically non-periodic configurations may be handled as well by prescribing values of the spatial periods L_x and L_y that are much larger than the dimensions of the contact surface.

5. Two-variable Fourier series

The steady state solution may be expressed using complex exponential Fourier series in the two variables x and y. Letting $f(x, y, z)$ be a generic physical quantity of the problem with $f \in \{ u, v, w, \epsilon_x, \epsilon_y, \epsilon_z, \gamma_{xy}, \gamma_{xz}, \gamma_{yz}, p, s_x, s_y, s_z, \tau_{xy}, \tau_{xz}, \tau_{yz}, \sigma_z \}$, its complex Fourier series expansion is written as

$$f(x, y, z) = \sum_{m,n=-\infty}^{+\infty} f_{mn}(z) e^{i\frac{2\pi m}{L_x}x} e^{i\frac{2\pi n}{L_y}y}, \tag{21}$$

where corresponding Fourier coefficients are defined by

$$f_{mn}(z) = \frac{1}{L_x L_y} \int_{y=0}^{L_y} \int_{x=0}^{L_x} f(x, y, z) e^{-i\frac{2\pi m}{L_x}x} e^{-i\frac{2\pi n}{L_y}y} dxdy. \tag{22}$$

Since $f(x, y)$ is real, $f_{m,-n} = \bar{f}_{-m,n}$ and $f_{-m,-n} = \bar{f}_{m,n}$, which reduces computational costs.

6. General solutions to Fourier coefficients

Substituting material coordinates for moving reference coordinates (i.e. $x = x' - V_s t$, $y = y'$ and $z = z'$) in expression (21) we may write

$$f(x', y', z', t) = \sum_{m,n=-\infty}^{+\infty} c_{mn}(x', y', z') e^{-i\frac{2\pi m}{L_x}V_s t}, \tag{23}$$

$$c_{mn}(x', y', z') = f_{mn}(z') e^{i\frac{2\pi m}{L_x}x'} e^{i\frac{2\pi n}{L_y}y'}, \tag{24}$$

and thus interpret that the material particles of the foundation (x', y', z') are subjected to an infinite sum of harmonic excitations to which, using the principle of superposition, the fundamental theory of viscoelasticity applies separately. Angular frequencies of individual harmonic movements are given by

$$\omega_m = -\frac{2\pi m}{L_x} V_s. \tag{25}$$

Identifying the generic quantity $f(x', y', z', t)$ with each component of stress ($\mathbf{s}$) and strain ($\boldsymbol{\epsilon}$) deviators, then applying the fundamental theory of viscoelasticity to each harmonic, while using the orthogonality property of complex exponentials, leads to the following relation between Fourier coefficient tensors

$$\mathbf{s}_{mn}(z) = 2G^*_m \boldsymbol{\epsilon}_{mn}(z), \tag{26}$$

where $G^*_m = G'(\omega_m) + iG''(\omega_m)$ is the dynamic shear modulus, $G'(\omega_m)$ and $G''(\omega_m)$ corresponding to the storage and loss moduli, respectively. The following shorthand parameters will be used in the sequel

$$\begin{aligned} &\nu_x = 2\pi m/L_x \; ; \; \nu_y = 2\pi n/L_y, \\ &\beta_x = (4\nu_x^2 + \nu_y^2)G^*_m - \rho V_s^2 \nu_x^2, \\ &\beta_y = (\nu_x^2 + 4\nu_y^2)G^*_m - \rho V_s^2 \nu_x^2, \\ &\beta_{xy} = 3\nu_x \nu_y G^*_m. \end{aligned} \tag{27}$$

Small strain complex Fourier coefficients are related to their deformation counterparts differentiating (21)

$$\epsilon_{x,mn}(z) = i\nu_x u_{mn}(z), \tag{28}$$

$$\epsilon_{y,mn}(z) = i\nu_y v_{mn}(z), \tag{29}$$

$$\epsilon_{z,mn}(z) = \dot{w}_{mn}(z), \tag{30}$$

$$\gamma_{xy,mn}(z) = i\nu_x v_{mn}(z) + i\nu_y u_{mn}(z), \tag{31}$$

$$\gamma_{xz,mn}(z) = i\nu_x w_{mn}(z) + \dot{u}_{mn}(z), \tag{32}$$

$$\gamma_{yz,mn}(z) = i\nu_y w_{mn}(z) + \dot{v}_{mn}(z). \tag{33}$$

where the up dot denotes the derivative with respect to z. Equilibrium equations are transformed into linear ordinary differential equations relating stresses to displacements, in terms of their respective Fourier coefficients, by plugging the generic Fourier expansion (21) into expression (8) and further using the orthogonality property of complex exponentials

$$-\rho V_s^2 \nu_x^2 u_{mn} = i\nu_x s_{x,mn} + i\nu_y \tau_{xy,mn} + \dot{\tau}_{xz,mn} - i\nu_x p_{mn}, \tag{34}$$

$$-\rho V_s^2 \nu_x^2 v_{mn} = i\nu_x \tau_{xy,mn} + i\nu_y s_{y,mn} + \dot{\tau}_{yz,mn} - i\nu_y p_{mn}, \tag{35}$$

$$-\rho V_s^2 \nu_x^2 w_{mn} = i\nu_x \tau_{xz,mn} + i\nu_y \tau_{yz,mn} + \dot{s}_{z,mn} - \dot{p}_{mn}. \tag{36}$$

Additional ODE's are obtained by substituting (28-33) into (26) in order to eliminate the strains

$$s_{x,mn} = 2i\nu_x G_m^* u_{mn}, \tag{37}$$

$$s_{y,mn} = 2i\nu_y G_m^* v_{mn}, \tag{38}$$

$$s_{z,mn} = 2G_m^* \dot{w}_{mn}, \tag{39}$$

$$\tau_{xy,mn} = iG_m^*(\nu_y u_{mn} + \nu_x v_{mn}), \tag{40}$$

$$\tau_{xz,mn} = G_m^*(\dot{u}_{mn} + i\nu_x w_{mn}), \tag{41}$$

$$\tau_{yz,mn} = G_m^*(\dot{v}_{mn} + i\nu_y w_{mn}). \tag{42}$$

A reduced number of six state variables is retained. The chosen state variables are ordered and stored in a complex-valued state vector $\mathbf{q}_{mn}(z)$, as follows

$$\mathbf{q}_{mn} = \left\langle w_{mn}, u_{mn}, v_{mn}, \sigma_{z,mn}, \tau_{xz,mn}, \tau_{yz,mn} \right\rangle^T. \tag{43}$$

Equations (34)-(42) are rearranged such that only the chosen state variables remain. The following system of linear ODE's is finally obtained

$$\dot{\mathbf{q}}_{mn} = \mathbf{A}_{mn}\mathbf{q}_{mn}, \tag{44}$$

where the complex valued matrix $\mathbf{A}_{mn}$ is given by

$$\mathbf{A}_{mn} = \begin{bmatrix} 0 & -i\nu_x & -i\nu_y & 0 & 0 & 0 \\ -i\nu_x & 0 & 0 & 0 & G_m^{*-1} & 0 \\ -i\nu_y & 0 & 0 & 0 & 0 & G_m^{*-1} \\ -\rho V_s^2 \nu_x^2 & 0 & 0 & 0 & -i\nu_x & -i\nu_y \\ 0 & \beta_x & \beta_{xy} & -i\nu_x & 0 & 0 \\ 0 & \beta_{xy} & \beta_y & -i\nu_y & 0 & 0 \end{bmatrix}. \tag{45}$$

The general solution to system (44) has the following form

$$\mathbf{q}_{mn}(z) = \mathbf{T}_{mn}(z)\mathbf{q}_{mn}(0) \text{ for } (0 \le z \le H), \tag{46}$$

where $\mathbf{T}_{mn}(z) = \exp(\mathbf{A}_{mn}z)$ is the complex matrix exponential of $\mathbf{A}_{mn}z$, which may be readily computed using mathematical software handling complex numbers. Alternatively, the following real valued system of double size may be solved

$$\begin{bmatrix} Re(\dot{\mathbf{q}}_{mn}) \\ -Im(\dot{\mathbf{q}}_{mn}) \end{bmatrix} = \begin{bmatrix} Re(\mathbf{A}_{mn}) & -Im(\mathbf{A}_{mn}) \\ Im(\mathbf{A}_{mn}) & Re(\mathbf{A}_{mn}) \end{bmatrix} \begin{bmatrix} Re(\mathbf{q}_{mn}) \\ -Im(\mathbf{q}_{mn}) \end{bmatrix}, \tag{47}$$

where $Re()$ and $Im()$ correspond, respectively, to the real and imaginary parts of a given quantity.

Displacement boundary conditions (i.e. $u_{mn}(0)$, $v_{mn}(0)$, $w_{mn}(0)$) are known at the bottom of the foundation strip while the boundary conditions on stresses (i.e. $\sigma_{z,mn}(H)$, $\tau_{xz,mn}(H)$, $\tau_{yz,mn}(H)$) result from the surface tractions applied on the contact surface. This two-point boundary value problem is solved by dividing the vector of unknowns $\mathbf{q}_{mn}$ into two subvectors:

$$\mathbf{q}_{mn}(z) = \left\langle \mathbf{d}_{mn}^T(z), \mathbf{f}_{mn}^T(z) \right\rangle^T, \tag{48}$$

where $\mathbf{d}_{mn}(z) = \langle w_{mn}(z), u_{mn}(z), v_{mn}(z)\rangle^T$ and $\mathbf{f}_{mn}(z) = \left\langle \sigma_{z,mn}(z), \tau_{xz,mn}(z), \tau_{yz,mn}(z)\right\rangle^T$, and writing solution (46) in the form

$$\begin{bmatrix} \mathbf{d}_{mn}(z) \\ \mathbf{f}_{mn}(z) \end{bmatrix} = \begin{bmatrix} \mathbf{T}_{mn,11}(z) & \mathbf{T}_{mn,12}(z) \\ \mathbf{T}_{mn,21}(z) & \mathbf{T}_{mn,22}(z) \end{bmatrix} \times \begin{bmatrix} \mathbf{d}_{mn}(0) \\ \mathbf{f}_{mn}(0) \end{bmatrix}. \tag{49}$$

Since $\mathbf{d}_{mn}(0) = \mathbf{0}$, rearranging expression (49) results in equation (50) relating the Fourier coefficients of displacements and stresses at $z = H$

$$\mathbf{d}_{mn}(H) = \mathbf{T}_{mn,12}(H)\mathbf{T}^{-1}_{mn,22}(H)\mathbf{f}_{mn}(H), \tag{50}$$

which opens the way to developing a boundary element formulation reflecting the foundation's behavior.

7. Boundary element formulation

Let K_x and K_y be the number of nodes discretizing the candidate contact surface, in directions x and y respectively, as illustrated in figure (2). The total number of nodes is hence $N_T = K_xK_y$. The boundary element compliance matrix $\mathbf{C}$ is defined by the constitutive equation

$$\begin{bmatrix} \mathbf{C}_{WW} & \mathbf{C}_{WU} & \mathbf{C}_{WV} \\ \mathbf{C}_{UW} & \mathbf{C}_{UU} & \mathbf{C}_{UV} \\ \mathbf{C}_{VW} & \mathbf{C}_{VU} & \mathbf{C}_{VV} \end{bmatrix} \times \begin{bmatrix} \mathbf{F}_W \\ \mathbf{F}_U \\ \mathbf{F}_V \end{bmatrix} = \begin{bmatrix} \mathbf{W} \\ \mathbf{U} \\ \mathbf{V} \end{bmatrix}, \tag{51}$$

where $\mathbf{F} = \left\langle \mathbf{F}_W^T, \mathbf{F}_U^T, \mathbf{F}_V^T \right\rangle^T$ and $\mathbf{D} = \left\langle \mathbf{W}^T, \mathbf{U}^T, \mathbf{V}^T \right\rangle^T$ correspond to the nodal displacement vector and the nodal force vector respectively, each subvector containing nodal components in a given direction. Nodal forces, applied at a given node N, are further associated with the corresponding surface traction using formulas that are similar to the one given below in the normal direction

$$\sigma_z^N(x, y, H) = \begin{cases} \frac{F_W^N}{a_x a_y}, & \text{if} \begin{cases} x^N - \frac{a_x}{2} \le x \le x^N + \frac{a_x}{2} \\ y^N - \frac{a_y}{2} \le y \le y^N + \frac{a_y}{2} \end{cases} \\ 0, & \text{otherwise.} \end{cases} \tag{52}$$

8. Building the compliance matrix

Entry $\mathbf{C}_{PQ}(M, N)$ of the compliance matrix $\mathbf{C}$ matches with the displacement in the direction corresponding to index "$P \in \{U, V, W\}$", at node M, when a unit force is applied at node N, in the direction corresponding to index "$Q \in \{U, V, W\}$". Hence in theory, the entries of matrix $\mathbf{C}$ may be obtained by applying unit forces, separately in each direction x, y and z and at each node, while determining the corresponding nodal displacements over the entire grid.

The computational cost of building compliance matrices increases quadratically with the number of discretization nodes and the truncation order. However, the cost can be reduced: in practice, provided that the spacings a_x and a_y between the nodes are uniform, in each of directions x and y, one may take advantage of configurational similarities such that less than six well-chosen columns of $\mathbf{C}$ need to be formed explicitly, by adding Fourier terms. Furthermore, depending on each problem's particular assumptions, mainly assumptions pertaining to friction along with the types of results that are specifically needed, building the entire compliance matrix may not be necessary. For instance, in applications where friction may be neglected one can set $\mathbf{F}_U = \mathbf{F}_V = \mathbf{0}$. Hence, provided that the horizontal displacements are not explicitly sought, only $1/9^{th}$ of the compliance matrix needs to be formed as (51) reduces to

$$\mathbf{C}_{WW}\mathbf{F}_W = \mathbf{W}. \tag{53}$$

Further details are given below on building relevant parts of the compliance matrix in a frictionless setting where only vertical unit forces need to be applied to appropriate nodes. Other parts of the compliance matrix may be obtained by following a very similar approach in the horizontal directions.

Letting i (from 1 to K_x) and j (from 1 to K_y) be the nodal indexes in directions of increasing x and y respectively, as shown in figure (2), a global node numbering may be obtained through the expression $N = (j-1)K_x + i$. With this numbering convention, unit vertical forces need only be applied to nodes number 1 and K_x. Indeed, if node couples

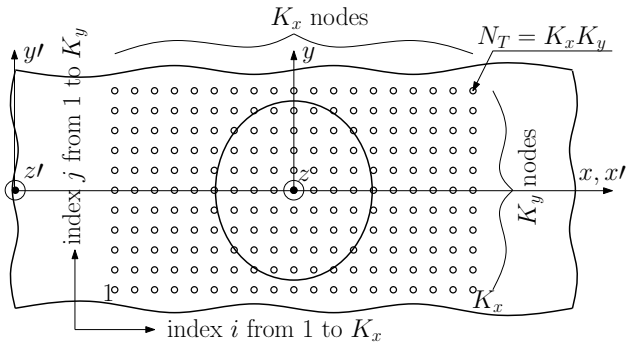

Figure 2: Discretization of the candidate contact surface

(M_1, N_1) and (M_2, N_2) have the same relative position, i.e. $(x_2^M - x_2^N) = (x_1^M - x_1^N)$ and $(y_2^M - y_2^N) = \pm(y_1^M - y_1^N)$, the vertical displacement of M_1 due to a vertical point load applied at N_1 will be the same as the displacement of M_2 when the load is applied at N_2. Note however that, due to motion along the x-axis, Oy is not an axis of symmetry. Hence, all other entries in matrices $\mathbf{C}_{WW}$, $\mathbf{C}_{UW}$ and $\mathbf{C}_{VW}$ can be deduced from columns 1 and K_x and therefore need not be formed by explicitly computing and adding Fourier terms. Similar considerations also apply to other submatrices of $\mathbf{C}$ in the case of frictional contact in 3D.

Implementing such configurational similarities in practice, drastically reduces the computational cost of building 3D compliance matrices as well as their storage space: both are divided by $N_T/2$. For instance, in the frictional example given in section 11, the candidate contact surface is discretized using $N_T = 41 \times 41 = 1681$ nodes, in which case, the computational cost of forming compliance matrices is roughly divided by 840. It takes for instance approximately 18 minutes (instead of days) using an Intel® Core™ i7 M620 CPU with 4 MB of cache memory and a clock speed of 2.66 GHz to compute a full 3D compliance matrix including $N_{tx} = N_{ty} = 500$ Fourier terms. Applying the same reasoning in two dimensions based on $N_T = 80$ nodes, the method presented by Qiu (2006) is rendered roughly 40 times more efficient.

By means of expression (52), a unit vertical force applied at a candidate contact node N is associated with the following normal traction

$$\sigma_z^N(x,y,H) = \begin{cases} \frac{1}{a_x a_y}, & \text{if} \begin{cases} x^N - \frac{a_x}{2} \le x \le x^N + \frac{a_x}{2} \\ y^N - \frac{a_y}{2} \le y \le y^N + \frac{a_y}{2} \end{cases} \\ 0, & \text{otherwise.} \end{cases} \tag{54}$$

The corresponding complex Fourier coefficients are obtained for relevant combination cases of m and n, using expression (22) in the following form

$$\sigma_{z,mn}(z) = \frac{1}{L_x L_y} \int_{y=0}^{L_y} \int_{x=0}^{L_x} \sigma_z(x,y,z) e^{-i\frac{2\pi m}{L_x}x} e^{-i\frac{2\pi n}{L_y}y} dxdy, \tag{55}$$

with the result given by

$$\sigma_{z,mn}^N(H) = \frac{\sin(\frac{\pi m a_x}{L_x})}{\pi m a_x} \frac{\sin(\frac{\pi n a_y}{L_y})}{\pi n a_y} e^{-i2\pi(\frac{m}{L_x}x^N + \frac{n}{L_y}y^N)}, \tag{56}$$

for $m \neq 0$ and $n \neq 0$. The remaining cases are

$$\sigma_{z,0n}^N(H) = \frac{e^{-i\frac{2\pi n}{L_y}y^N}}{\pi n L_x a_y} \sin(\frac{\pi n a_y}{L_y}) \text{ for } m = 0 \text{ and } n \neq 0, \tag{57}$$

$$\sigma_{z,m0}^N(H) = \frac{e^{-i\frac{2\pi m}{L_x}x^N}}{\pi m L_y a_x} \sin(\frac{\pi m a_x}{L_x}) \text{ for } m \neq 0 \text{ and } n = 0, \tag{58}$$

$$\sigma_{z,00}^N(H) = \frac{1}{L_x L_y} \text{ for } m = 0 \text{ and } n = 0. \tag{59}$$

It is now possible to determine Fourier coefficients for the displacements using expression (50). We hence write

$$\mathbf{f}_{mn}(H) = \left\langle \sigma^N_{z,mn}(H), 0, 0 \right\rangle^T, \tag{60}$$

$$\mathbf{d}^N_{mn}(H) = \left\langle w^N_{mn}(H), u^N_{mn}(z), v^N_{mn}(z) \right\rangle^T = \mathbf{T}_{mn,12}(H)\mathbf{T}^{-1}_{mn,22}(H)\mathbf{f}^N_{mn}(H). \tag{61}$$

Corresponding Fourier terms are finally assembled into the entries of the relevant compliance submatrix. In this case

$$\mathbf{C}_{WW}(M,N) = \sum_{m,n=-\infty}^{+\infty} w^N_{mn}(H) e^{i\frac{2\pi m}{L_x}x^M} e^{i\frac{2\pi n}{L_y}y^M}. \tag{62}$$

9. Solving the rolling contact problem

At this point both physical entities have been modeled, i.e. described in mathematical terms. The behavior of the viscoelastic layer, in the moving frame of reference, is comprehensively depicted by the boundary element formulation given by equation (51) while the hard rolling object is fully described by its lower geometrical profile (13).

Solving the rolling contact problem mainly involves the implementation of normal and tangential contact boundary conditions as given by sets of equations (11)-(12) and (16)-(18), respectively. As performed by Qiu (2006) in a two-dimensional context, while implementing the tangential boundary conditions, specific constraints are imposed on the stick-contact nodes such that the absence of relative motion is satisfied in regions of sticky contact. Because V_s and Ω are global constants, it can be derived from (14) and (15) that $\frac{\partial u}{\partial x}(x, y, H)$ and $v(x, y, H)$ remain both constant across stick-contact zones, in each plane of constant y. Continuity of these fields, in direction x, is imposed across leading edge stick-contact nodes.

Nonlinear constraints resulting from contact problems are usually difficult to model. They may be enforced using FEM schemes as detailed, for instance, in Oden and Lin (1986) or Zienkiewicz and Taylor (2005). Alternatively, Zéhil and Gavin (2013a) describe a relatively simple solving strategy for frictional rolling contact problems in two and three dimensions. The latter is used in its 3D version for the purposes of this work in order to determine the problem unknowns: (i) the vertical forces acting on all contact nodes, (ii) the horizontal forces acting on stick-contact nodes, (iii) the vertical displacements of the free nodes, (iv) the horizontal displacements of all the nodes, (v) the indentation d and (vi) the rotational speed Ω. Rolling resistance (1) may finally be computed according to the following expression

$$R_r = \sum \mathbf{F}_U + \frac{T\Omega}{V_s}. \tag{63}$$

In the example of section 11, rolling resistance results *with* and *without* surface friction are compared. The results *without* friction were obtained using a reduced version of the contact solver, based on equation (53) derived by setting $F_U = F_V = 0$ (see section 8), and on vertical equilibrium. In such cases, the rotational quantities T and Ω are indeterminate and the rolling resistance writes $\bar{R}_r = -\mathbf{x}^T\mathbf{F}_W/R$, where $\mathbf{x}$ is the nodal vector of x-coordinates.

10. Verification examples

In the present section, the three-dimensional model is tested in elastic and stationary conditions. The results are compared with those given by Jaffar (2008) and Jaffar (1997) for thick and thin foundation layers respectively.

10.1. Thick foundation

The stationary contact of a rigid sphere with an elastic layer of finite thickness H was examined by Jaffar (2008) in frictionless conditions. It was found that, for a relatively thick foundation strip in comparison with the contact radius r_c (i.e. $\gamma = r/r_c \leq 0.9$) the contact pressure distribution followed the form given by Hertz, i.e.

$$\sigma_z(r) = \frac{3P}{2\pi r_c^2}\sqrt{1 - \left(\frac{r}{r_c}\right)^2}, \tag{64}$$

while the contact radius was given by the following expression

$$r_c = \left[\frac{PRD(1-\nu)}{8\pi G}\right]^{\frac{1}{3}}, \tag{65}$$

where G and ν are the shear modulus and Poisson's ratio respectively and D is defined as follows

$$D = 3\pi + 8\gamma^3\left(b_1 + \frac{2}{5}b_2\gamma^2\right), \tag{66}$$

with coefficients b_m expressed (for $m = 1, 2$) as

$$b_m = \left(-\frac{1}{4}\right)^m \int_0^\infty (1 - L(\omega))\,\omega^{2m} d\omega. \tag{67}$$

For a foundation bonded to its substrate $L(w)$ is given by

$$L(\omega) = \frac{2\kappa\sinh(2\omega) - 4\omega}{2\kappa\cosh(2\omega) + 4\omega^2 + \kappa^2 + 1}, \text{ with } \kappa = 3 - 4\nu. \tag{68}$$

In order to simulate conditions by which the above estimates apply, we consider the case of a rigid sphere of radius $R = 2$ cm in stationary ($V_s = 0$ m/s) and frictionless ($\mu = 0$) contact with an elastic layer ($G'(\omega) = G_0 = 3.0$ MPa ; $G''(\omega) = 0$ MPa) of thickness $H = 5$ mm. A vertical load of $P = 100$ N is applied to the sphere. The periodic lengths are set to $L_x = L_y = 20$ cm and the nodal spacings are taken equal to $a_x = a_y = 0.25$ mm. The truncation orders are set to $N_{t_x} = N_{t_y} = 2000$.

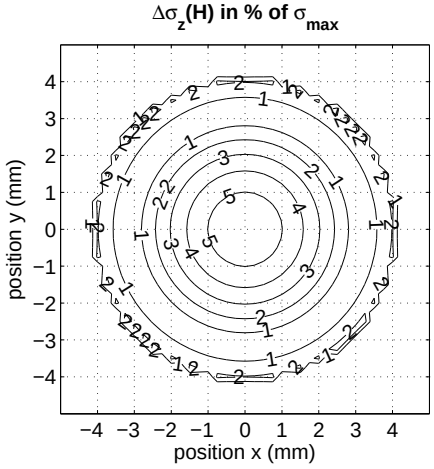

Figure 3: Relative difference between model and asymptotic pressure fields for $H = 5$mm

The contact radius resulting from the 3D model is of 4.5 ± 0.125 mm, which is compatible with the one given by solving (65) and (66) i.e. 4.56 mm. Figure 3 shows a contour plot of the difference between pressure fields, which does not exceed $\approx 5\%$ of the maximum pressure at the center σ_{max}. Given the current precision settings on the 3D model and the fact that (66) corresponds to a truncated quantity, the comparison is quite satisfactory. Note that minor irregularities in the vicinity of the outer contour arise from the fact that the rectangular grid cannot perfectly match the circular shape of the contact area while both pressure profiles are rapidly changing: referring to equation (64), it can be shown that $|d\sigma_z(r)/dr| \to \infty$ as $r \to r_c$.

10.2. Thin foundation

Jaffar (1997) provides an asymptotic solution to the stationary contact problem of a rigid sphere with a thin elastic and incompressible foundation at the distinguished limit $\epsilon = r_c/H \to 0$. In this case, the contact pressure takes the

following form

$$\sigma_z(r) = \frac{3P}{\pi r_c^2}\left(1 - \left(\frac{r}{r_c}\right)^2\right)^2, \tag{69}$$

while the contact radius r_c may be expressed as

$$r_c = \left[\frac{48PRH^3}{\pi G(1+\nu)}\right]^{\frac{1}{6}}. \tag{70}$$

Taking the same parameters as in 10.1, the foundation's thickness is reduced to $H = 0.1$ mm and the sphere's radius increased to $R = 80$ m so that a relatively large contact radius can be obtained. A vertical load of $P = 10$ N is applied to the sphere.

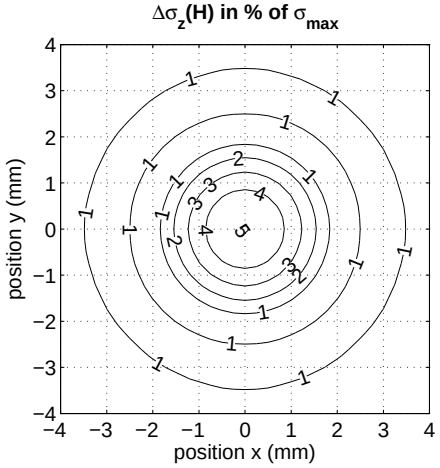

Figure 4: Relative difference between model and asymptotic pressure fields for $H = 0.1$mm

The contact radius resulting from the 3D model is of 3.75 ± 0.125 mm, which is compatible with the solution given by (70) i.e. 3.7 mm. The contour plot in figure 4 shows that the difference between pressure fields remains below $\approx 5\%$ of σ_{max}. The comparison is satisfactory given the finite precision of the 3D model and the fact that (69) corresponds to an asymptotic solution.

11. Example of rolling with friction

11.1. Default parameters

Referring to equation (4) in section 2, let us consider a rigid sphere of radius $R = 2$ cm driven by a horizontal force Q applied at the top. A concomitant vertical load of $P = 150$ N is applied at the center. The sphere is rolling with friction ($\mu = 0.2$), in steady state, at a linear speed $V_s = 0.05$ m/s on a viscoelastic layer of thickness $H = 5$ mm and density $\rho = 1000$ kg/m^3.

For illustrative purposes the foundation's material is modeled by a three-parameter viscoelastic solid (see figure 5) whose master curves are given by

$$\begin{aligned} G'(\omega) &= G_0(1+f)\frac{(1+f)+\omega^2\tau^2}{(1+f)^2+\omega^2\tau^2}, \\ G''(\omega) &= G_0(1+f)\frac{f\omega\tau}{(1+f)^2+\omega^2\tau^2}. \end{aligned} \tag{71}$$

where $G_o = G'(0) = (G_1G_2)/(G_1+G_2) = 3.0$ MPa is the static shear modulus, $\tau = \eta/G_2 = 0.25$ s is the creep time and $f = G_1/G_2 = 1$.

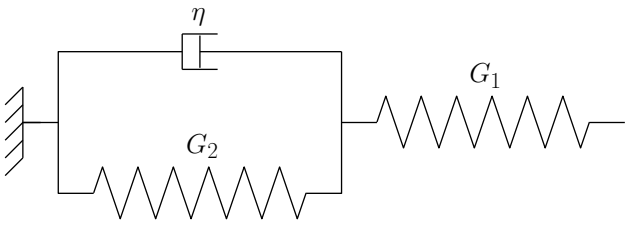

Figure 5: Three-parameter viscoelastic solid

The spatial periods are set to $L_x = L_y = 20$ cm which, up to a speed of about 50 cm/s, is large enough to allow for sufficient (i.e. more than 80%) creep recovery of the foundation layer between two successive sphere arrivals. Based on the convergence results of table 1, nodal spacings are set equal to $a_x = a_y = 0.25$ mm and truncation orders of $N_{t_x} = N_{t_y} = 2000$ are retained for the main calculations. Figures that require building multiple compliance matrices are drawn using $N_{t_x} = N_{t_y} = 500$, which is sufficient for plotting purposes.

In following subsections, two cases are compared: (i) a *frictional* case corresponding to the rolling speed V_s, the vertical load P and the driving torque $T = QR$, and (ii) a *frictionless* case characterized by the same rolling speed V_s and vertical load P. For illustration purposes, some of the parameters introduced in this subsection will be changed in the following ones, depending on the topic requirements.

11.2. General results

Figure 6 shows a contour plot of the vertical stress field $\sigma_z(x, y, z = H)$ over the contact area. The observed dissymmetry is mainly due to the viscoelastic behavior of the foundation layer and is responsible for the viscoelastic rolling resistance.

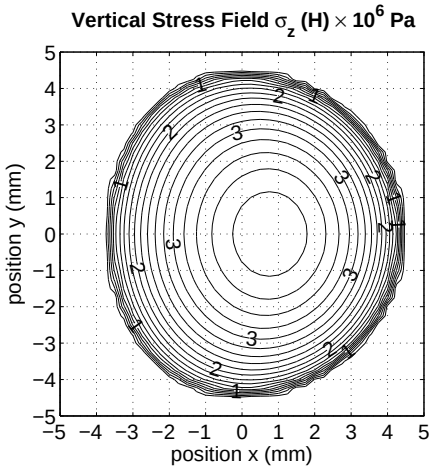

Figure 6: General results of the 3D model: vertical stress field $\sigma_z(x, y, H)$

The rolling resistance is computed according to equations (2)-(4) which in this case yield a total rolling resistance of $R_r = 3.07$ N, from which less than 0.05 N originate from slipping friction.

11.3. Convergence table

In order to verify convergence, the rolling resistance was evaluated in frictionless conditions using the same nodal spacing in both directions (i.e. $a = a_x = a_y$) varying from 0.15 to 1 mm and the same truncation order in both spatial frequencies (i.e. $N_t = N_{t_x} = N_{t_y}$) ranging from 500 to 3000 terms. The resulting values are reproduced in table 1 and fall within 3.4% of each other. It may furthermore be noted that, when the node spacing is less than or equal to 0.30 mm, the results are well within 0.2%, which is suitable for most engineering applications.

a (mm)	Truncation order N_t (Number of Terms)					
	500	1000	1500	2000	2500	3000
1.00	3.1129	3.1131	3.1135	3.1133	3.1135	3.1135
0.50	3.0138	3.0130	3.0130	3.0130	3.0130	3.0131
0.30	3.0212	3.0208	3.0206	3.0207	3.0206	3.0207
0.25	3.0259	3.0255	3.0257	3.0257	3.0257	3.0257
0.20	3.0252	3.0251	3.0255	3.0256	3.0255	3.0254
0.15	N/A	3.0258	3.0257	3.0257	3.0257	3.0257

Table 1: Effects of nodal spacing and truncation order on convergence

	H = 5 mm (r^2 = 0.9999)		H = 30 mm (r^2 = 1)[1]	
	Lower bound	Upper bound	Lower bound	Upper bound
a_p	2.701×10^{-3}	3.056×10^{-3}	2.554×10^{-3}	2.701×10^{-3}
b_p	1.381	1.407	1.510	1.521

Table 2: Power fitting coefficients for $R_r(P)$ - 95% confidence intervals

[1] r^2 is the square of the multiple correlation coefficient

	P = 50 N (r^2 = 0.9999)		P = 125 N (r^2 = 1)	
	Lower bound	Upper bound	Lower bound	Upper bound
a_e	0.9306	0.9403	3.738	3.768
b_e	1.555	1.954	1.706	2
c_e	-0.8799	-0.8555	-3.704	-3.662
d_e	-233	-223.2	-198.6	-193.8

Table 3: Exponential fitting coefficients for $R_r(H)$, 95% confidence intervals

11.4. Influence of the vertical load

Variations of the rolling resistance with respect to the vertical load, for H = 5 mm and H = 30 mm, are plotted on figures 7(a) and 7(b) respectively. Both cases, with and without friction, are considered. The resulting curves are concave upwards and are very similar in shape to the example given by Qiu (2006) corresponding to a two-dimensional model of a rigid cylinder rolling on a viscoelastic foundation.

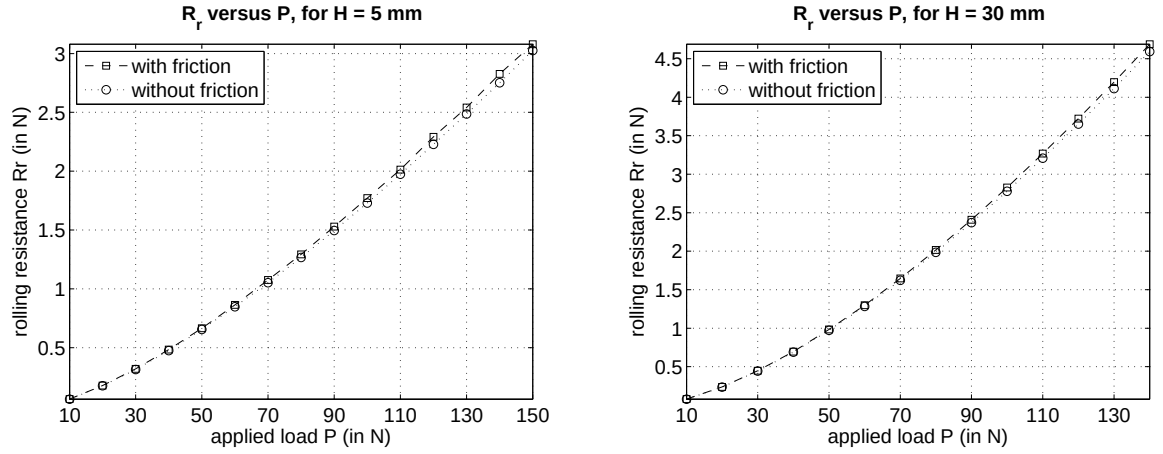

(a) R_r versus P, for H = 5 mm

(b) R_r versus P, for H = 30 mm

Figure 7: Influence of the vertical load on the rolling resistance

The rolling resistance increases monotonically with the applied load. Curves from figure 7 may be closely fitted using a power law of the form $R_r = a_p P^{b_p}$. In the cases including friction, the 95% confidence intervals on coefficients a_p and b_p are given in table 2.

11.5. Influence of the foundation's thickness

Variations of the rolling resistance with respect to the foundation's thickness, for P = 50 N and P = 125 N are plotted on figures 8(a) and 8(b) respectively. Both cases, with and without friction, are also considered. As expected, the resulting curves are concave downwards and converge asymptotically towards a limiting case corresponding to a viscoelastic "half-space", at the given speed.

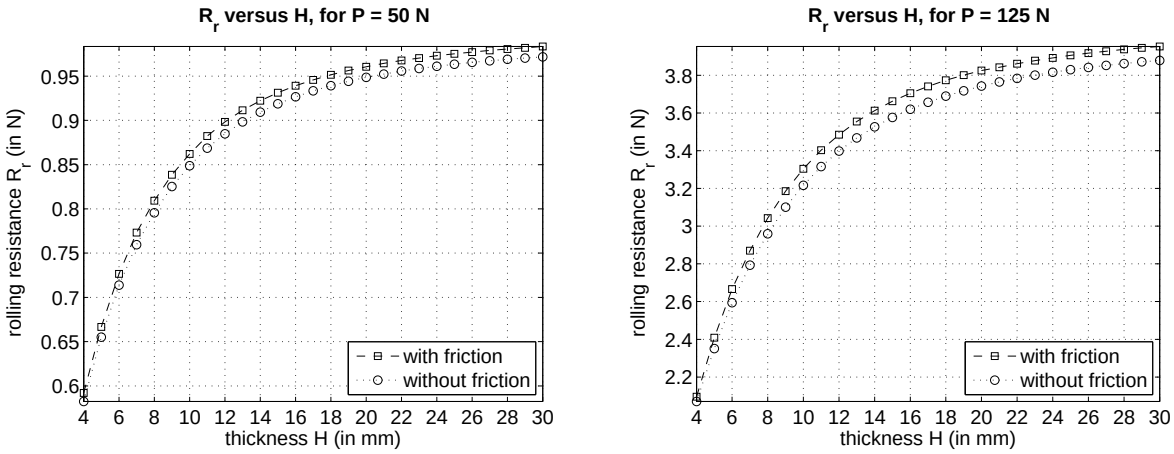

(a) R_r versus H, for $P = 50$ N

(b) R_r versus H, for $P = 125$ N

Figure 8: Influence of the foundation's thickness on the rolling resistance

The rolling resistance is a monotonically increasing function of the layer thickness. Curves from figure 8 may be closely fitted using an exponential law of the form $R_r = a_e \exp^{b_e P} + c_e \exp^{d_e P}$. In the case including friction, the 95% confidence intervals on coefficients a_e, b_e, c_e and d_e are given in table 3.

11.6. Influence of friction

In section 11.2 we mentioned that the rolling resistance due to friction was small in comparison with the one resulting from viscoelasticity. Two curves for $R_r(P)$, with and without friction, were compared on each of figures 7(a) and 7(b) for $H = 5$ mm and $H = 30$ mm respectively. The influence of friction was also highlighted by comparing two curves for $R_r(H)$ on each of figures 8(a) and 8(b), for $P = 50$ N and $P = 125$ N respectively [2]. It may be noted that, for values of P up to 150 N (corresponding to a mean vertical pressure of 2.56 MPa), the contribution of friction remains below 1.55%, which suggests that it may be neglected for many engineering applications.

Friction losses vary with the different parameters but remain relatively small. For instance, the dependence upon the foundation's thickness of their percentage contribution to rolling resistance, is illustrated in figures 9(a) and 9(b) for $P = 50$ N and $P = 125$ N respectively. Data points present minor discontinuities due to the spatial discretization of slipping, which is a continuous process across the contact area. Indeed, in the model, changes in contact nature can only occur over surface elements of area $a_x \times a_y$. Considering the limited influence of friction on the rolling resistance, fitting the available data points was deemed more cost efficient than refining the mesh. In both cases of vertical loading, it can be seen that the contribution of friction to the total rolling resistance reaches a maximum for layer thickness between 6 and 8 mm.

11.7. Influence of speed

The dependence of rolling resistance upon linear speed is perhaps the most important in that it more directly reflects the time dependent behavior of the viscoelastic foundation. Using various approximations, its main features were commendably approached for instance by May et al. (1959) and Pőschel et al. (1999) in the case of a hard cylinder and more recently by Persson (2010) for both rigid cylinders and spheres on a viscoelastic foundation. Plots of $R_r(V_s)$ are shown in figures 10(a)-(b), for different values of the vertical load ($10 \leq P \leq 150$ N) and two layer thicknesses ($H = 1$,and 30 mm).

Referring to the three-parameter model drawn in figure 5, viscoelastic energy dissipation only occurs in the dash-pot. Besides, the material's internal clocks are defined by its creep time τ and its relaxation time $\tau_r = \tau/(1+f)$ which,

[2] $P = 50$ and 125 N correspond to mean vertical pressures of 1.64 and 2.35 MPa respectively

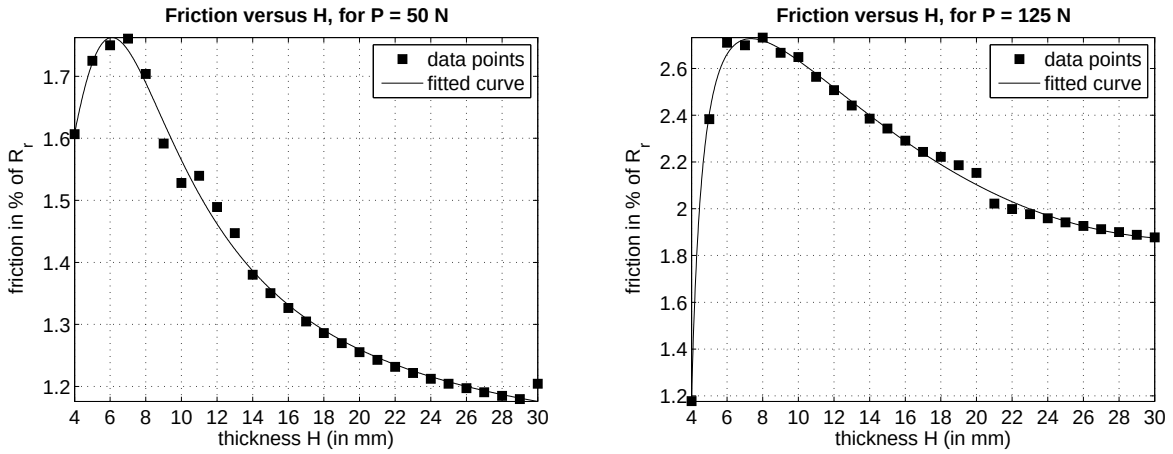

(a) Friction in % of R_r, for P = 50 N

(b) Friction in % of R_r, for P = 125 N

Figure 9: Percentage contribution of friction to the rolling resistance

in the case of our example, are of the same order of magnitude and therefore constitute a single time scale. According to this time scale, when the sphere is moving slowly (stationary limit), the dashpot flows and the layer behaves like an elastic spring of stiffness G_o. Conversely, when the sphere rolls rapidly, the dashpot locks and the foundation behaves also elastically, with stiffness E_1. Hence at low and high speeds, viscoelastic energy losses are expected to be small. The dashpot dissipates more energy at intermediate motion velocities, yielding a maximum rolling resistance depending on the problem's parameters, in particular the foundation's relaxation spectrum.

12. Conclusions

A three-dimensional boundary element formulation of an incompressible, linear viscoelastic layer of finite thickness was proposed, in a frame of reference moving at constant speed. The constitutive behavior of the layer's material is characterized, in the frequency domain, using general master-curves, which allows any linear viscoelastic model, including fully experimental results. The presented developments resulted in the formation of a compliance matrix characterizing the mechanical behavior of the layer's upper boundary and including the effects of steady-state motion. Such representation eliminates the need to model the entire layer and avoids any related artefacts on the lateral boundaries. As opposed to certain existing approaches, the proposed formulation does not rely on the elastic half-space approximation and poses no limitations regarding how thin the layer can be. The stresses and strains resulting from the boundary's interaction with its environment are propagated into the layer's continuum 'exactly', according to linear viscoelasticity. The proposed formulation can be used as a component in various settings, such as problems involving deformable indenters, multilayered contact or bifurcation and standing-wave phenomena. Taking advantage of configurational similarities and symmetry, the full computational cost and storage space of compliance matrices were divided by $N_T/2$. Furthermore, it is noteworthy that, for a given rolling/sliding speed, the compliance matrix of a viscoelastic layer needs to be built once and can be stored for multiple use. For instance, varying parameters such as the intensity of the applied loads, the coefficient of surface friction, the adhesion threshold, the shape or the dimensions of the indenter does not require re-forming the compliance matrix of the layer. The proposed formulation is hence suitable for efficiently generating sequences of high fidelity solution results for various quantities of interest, such as rolling resistance. In this work, it was implemented, in combination with a contact solver, to build a full three-dimensional model for the resistance incurred by a rigid sphere rolling or sliding on the layer. Energy losses include viscoelastic damping and surface friction. Responses from the model in limiting cases were found to be consistent with existing solutions. In order to illustrate some of the model's capabilities, an example was treated in which the foundation is described by a three-parameter viscoelastic solid and friction is assumed to follow Coulomb's law. Results from the example were used to illustrate the influence of vertical loading, foundation thickness, friction and

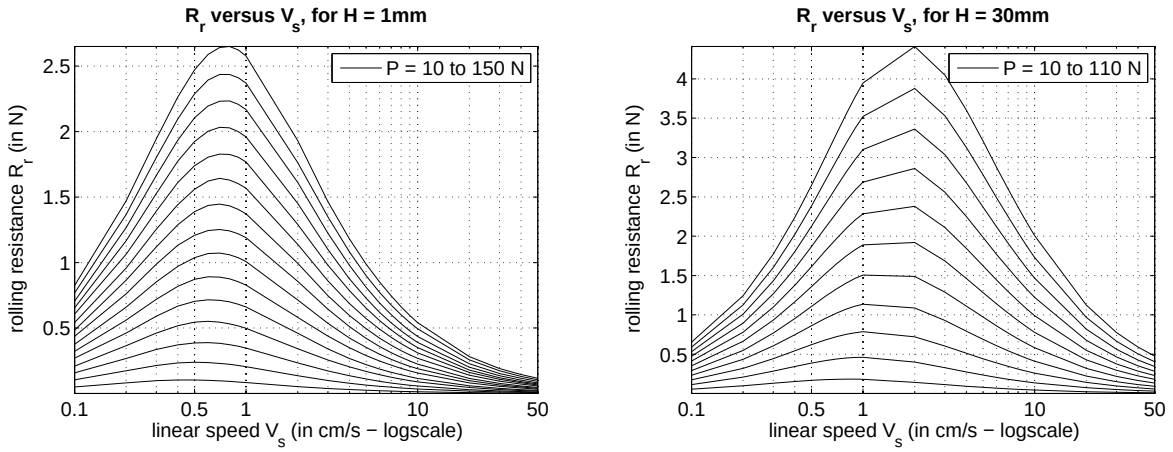

(a) R_r versus V_s, for $H = 1$ mm

(b) R_r versus V_s, for $H = 30$ mm

Figure 10: Influence of speed on the rolling resistance

speed on the rolling resistance. Some general aspects of previously-described dependences based on two-dimensional models in plane strain for rolling cylinders or simplified approaches for spheres were confirmed. In particular, the contribution of surface friction to the total rolling resistance was found to be limited. Energy losses increase unboundedly with vertical loading on which the dependency is fitted well by power laws. Rolling resistance also increases with foundation thickness but tends asymptotically towards a limiting case corresponding to a viscoelastic "half-space" solution. Alternatively, frictional losses were found to first increase then decrease with foundation thickness. Finally, starting from rest, viscoelastic dissipation grows with the rate of motion reaching a maximum that depends on the problem's parameters, then decays to become negligible at high speed.

Acknowledgments

This material is based upon work supported by the National Science Foundation under Grant No. NSF-CMMI-0900324. Any opinions, findings, and conclusions or recommendations expressed in this material are those of the authors and do not necessarily reflect the views of the National Science Foundation.

References

Barber, J., Ciavarella, M., Afferrante, L., Sackfield, A., 2008. Effect of small harmonic oscillations during the steady rolling of a cylinder on a plane. International Journal of Mechanical Sciences 50 (9), 1344–1353.

Brilliantov, N. V., Pőschel, T., 1998. Rolling friction of a viscous sphere on a hard plane. Europhysics Letters 42, 511–516.

Chertok, D. L., Golden, J. M., Graham, G. A. C., 2001. Hysteretic friction for the transient rolling contact problem of linear viscoelasticity. Journal of Applied Mechanics 68 (4), 589–595.

Coulomb, C., 1821. Théorie des machines simples: en ayant égard au frottement de leurs parties et à la roideur des cordages. Bachelier.

Flom, D. G., Bueche, A. M., 1959. Theory of rolling friction for spheres. Journal of Applied Physics 30 (11), 1725–1730.

Flügge, W., 1975. Viscoelasticity. Springer-Verlag.

Galin, L., Gladwell, G., 2008. Contact Problems: The Legacy of L.A. Galin. Solid Mechanics and Its Applications. Springer.

Golden, J., Graham, G., 2001. The problem of a viscoelastic cylinder rolling on a rigid half-space. Mathematical and Computer Modelling 34 (12–13), 1363–1397.

Greenwood, J. A., Minshall, H., Tabor, D., 1961. Hysteresis losses in rolling and sliding friction. Proceedings of the Royal Society of London. Series A, Mathematical and Physical Sciences 259 (1299), 480–507.

Hall, D. E., 2001. Fundamentals of rolling resistance. Rubber Chemistry and Technology 74 (3), 525–525.

Hunter, S., 1961. The rolling contact of a rigid cylinder with a viscoelastic half space. Journal of Applied Mechanics 28 (4), 611–617.

Jaffar, M., 1997. A general solution to the axisymmetric frictional contact problem of a thin bonded elastic layer. Proceedings of the Institution of Mechanical Engineering 211 (7), 549–558.

Jaffar, M., 2008. On the frictionless axi-symmetric contact of a thick elastic layer and the associated squeeze film problem. Proceedings of the Institution of Mechanical Engineering Part J, Journal of Engineering Tribology 222 (1), 61–68.

Johnson, K., 1985. Contact mechanics. Cambridge University Press, Cambridge.

Lakes, R., 2009. Viscoelastic Materials. Cambridge University Press.

Laursen, T. A., Stanciulescu, I., 2006. An algorithm for incorporation of frictional sliding conditions within a steady state rolling framework. Communications in Numerical Methods in Engineering 22 (4), 301–318.

Lee, W., Cho, K., Jang, H., 2009. Molecular dynamics simulation of rolling friction using nanosize spheres. Tribology Letters 33, 37–43.

May, W. D., Morris, E. L., Atack, D., 1959. Rolling friction of a hard cylinder over a viscoelastic material. Journal of Applied Physics 30 (11), 1713–1724.

Morland, L. W., 1967. Exact solutions for rolling contact between viscoelastic cylinders. The Quarterly Journal of Mechanics and Applied Mathematics 20 (1), 73–106.

Morland, L. W., 1968. Rolling contact between dissimilar viscoelastic cylinders. The Quarterly Journal of Mechanics and Applied Mathematics 25 (4), 363–376.

Munisamy, R., Hills, D., Nowell, D., 1991. Brief note on the tractive rolling of dissimilar elastic cylinders. International Journal of Mechanical Sciences 33 (3), 225–228.

Oden, J., Lin, T., 1986. On the general rolling contact problem for finite deformations of a viscoelastic cylinder. Computer Methods in Applied Mechanics and Engineering 57 (3), 297–367.

Persson, B., 2010. Rolling friction for hard cylinder and sphere on viscoelastic solid. The European Physical Journal E Soft Matter 33 (4), 327–33.

Pőschel, T., Schwager, T., Brilliantov, N., 1999. Rolling friction of a hard cylinder on a viscous plane. The European Physical Journal B - Condensed Matter and Complex Systems 10, 169–174.

Qiu, X., 2006. Full two-dimensional model for rolling resistance: hard cylinder on viscoelastic foundation of finite thickness. Journal of Engineering Mechanics 132 (11), 1241–1251.

Qiu, X., 2009. Full two-dimensional model for rolling resistance. ii: Viscoelastic cylinders on rigid ground. Journal of Engineering Mechanics 135 (1), 20–30.

Sharp, A., 2009. Rolling resistance: Part 1 of fuel consumption. Fleet Equipment 35 (11), 10–10.

Stanciulescu, I., Laursen, T. A., 2006. On the interaction of frictional formulations with bifurcation phenomena in hyperelastic steady state rolling calculations. International Journal of Solids and Structures 43 (10), 2959–2988.

Tabor, D., 1955. The mechanism of rolling friction. ii. the elastic range. Proceedings of the Royal Society of London. Series A, Mathematical and Physical Sciences 229 (1177), 198–220.

Vince, S., Shepherd, A., 1785. On the motion of bodies affected by friction. Philosophical Transactions of the Royal Society of London 75, 165–189.

Wang, G., Knothe, K., 1993. Stress analysis for rolling contact between two viscoelastic cylinders. Journal of Applied Mechanics 60 (2), 310–317.

Zéhil, G.-P., Gavin, H. P., 2013a. Simple algorithms for solving steady-state frictional rolling contact problems in two and three dimensions. International Journal of Solids and Structures 50 (6), 843 – 852.
URL `http://www.sciencedirect.com/science/article/pii/S0020768312004921`

Zéhil, G.-P., Gavin, H. P., 2013b. Simplified approaches to viscoelastic rolling resistance. International Journal of Solids and Structures 50 (6), 853 – 862.
URL `http://www.sciencedirect.com/science/article/pii/S002076831200409X`

Zienkiewicz, O. C., Taylor, R. L., Sep. 2005. The Finite Element Method for Solid and Structural Mechanics, 6th Edition. Butterworth-Heinemann.